Journal of Alloys and Compounds 509 (2011) 7488–7492

Contents lists available at ScienceDirect

Journal of Alloys and Compounds

journal homepage: www.elsevier.com/locate/jallcom

Spectroscopic investigation of Er^{3+}-doped $(Gd_{0.7}Y_{0.3})_2SiO_5$ single crystal for potential application in 1.5 μm laser

Yuchong Ding[a,b,*], Guangjun Zhao[a], Yosuke Nakai[c], Taiju Tsuboi[c]

[a] Key Laboratory of Materials for High Power Laser, Shanghai Institute of Optics and Fine Mechanics, Chinese Academy of Sciences, Shanghai 201800, China
[b] Graduate School of Chinese Academy of Sciences, Beijing 100039, China
[c] Faculty of Engineering, Kyoto Sangyo University, Kamigamo, Kita-ku, Kyoto 603-8555, Japan

ARTICLE INFO

Article history:
Received 15 February 2011
Received in revised form 15 April 2011
Accepted 16 April 2011
Available online 23 April 2011

Keywords:
Optical materials
Crystal growth
Optical spectroscopy
Luminescence

ABSTRACT

The Er^{3+}:$(Gd_{0.7}Y_{0.3})_2SiO_5$ (hereafter abbreviated as Er^{3+}:$G_{0.7}Y_{0.3}SO$) single crystals were grown by the Czochralski technique. The unpolarized absorption spectrum and photoluminescence (PL) spectra were measured at room temperature. The Judd–Ofelt phenomenological method was used to estimate the intensity parameters, radiative lifetimes and branching ratios of luminescence. The stimulated emission cross-section of the $^4I_{13/2} \rightarrow {}^4I_{15/2}$ transition of special interest of ~1.5 μm laser was calculated by the Fuchtbauer–Ladenburg equation, and the relevant gain cross-sections were also estimated for several inverse-population parameters to evaluate a potential laser activity of the Er^{3+}:$G_{0.7}Y_{0.3}SO$ system. Also, the potential range of the optical pumping was assessed based on the absorption cross-section at room temperature. Finally the excited state dynamics of the Er^{3+}:$G_{0.7}Y_{0.3}SO$ system was investigated and experimental lifetimes of $^4I_{13/2}$ and $^4I_{11/2}$ levels were measured. Taking into account the satisfactory absorption near 971 and 1529 nm, and the high gain cross-section in the range of 1530–1620 nm, the Er^{3+}:$G_{0.7}Y_{0.3}SO$ crystal can be considered as a promising active material for laser operation near 1.5 μm.

1. Introduction

The search for new diode pumped laser materials emitting around 1.5 μm becomes high interest, due to their numerous applications in eyesafe range finding, nonlinear optics and optical fiber telecommunications [1]. Emission in the 1.5 μm range can be achieved with Er^{3+} ions through the $^4I_{13/2} \rightarrow {}^4I_{15/2}$ transition. Er^{3+} laser systems can be pumped by the commercially available InGaAs (~980 nm) or InP (~1530 nm) laser diodes (LD), and such laser oscillations have been observed with several crystalline laser hosts, for instance, in YAG [2], LuAG [3] or silicate [4–7] compounds.

Of various hosts including silicates, the solid–solution of oxyorthosilicates have attracted many researchers' attentions owing to their peculiarity of disordered structure which would result in advantageous inhomogeneous broadening of the absorption and emission bands, thereby improving pumping efficiency as well as providing broader laser tunable range and ability to produce short laser pulses. The crystal structures and spectroscopic properties of Re^{3+} doped GYSO and LYSO are well documented [8,9], and the efficient cw tunable laser applying Yb^{3+}:GYSO system are already realized [10]. In the view of such advantages of solid solutions mentioned above, Er^{3+}:GYSO single crystal is also considered as a promising material to obtain efficient ~1.5 μm laser.

In this work, an Er^{3+} doped $(Gd_{0.7}Y_{0.3})_2SiO_5$ (hereafter abbreviated as $G_{0.7}Y_{0.3}SO$) single crystal was grown by the Czochralski method and its spectroscopic properties including absorption and photoluminescence (PL) spectra were reported. The absorption abilities of the Er^{3+}:$G_{0.7}Y_{0.3}SO$ crystals were evaluated especially with optical pumping ranges and the relaxation dynamics of excited states were studied. Thereby, the spectroscopic parameters relevant to assess the potential laser activity of the Er^{3+}:$G_{0.7}Y_{0.3}SO$ system were determined and discussed.

2. Experimental

Single crystals of solid solutions with intentional stoichiometry $G_{0.7}Y_{0.3}SO$ were grown by the Czochralski method from iridium crucibles. The Er^{3+} doping concentration is chosen to be 0.5 at.% with respect to Gd^{3+} to suppress the upconversion possibility occurring at $^4I_{11/2} \rightarrow {}^4S_{3/2}$ ($^2H_{11/2}$) or $^4I_{13/2} \rightarrow {}^4I_{9/2}$. A 30 kW pillar power generator with maximum frequency of 10 kHz was used as power supply and an EUROTHERM 3504 was used to control the diameter exactly by monitoring the weight of the crucible. The starting materials with high purity (≥99.999%) were appropriately dried and weighed according to the formula $(Er_{0.005}Gd_{0.695}Y_{0.3})_2SiO_5$.

After the compounds were ground and mixed, they were pressed into tables with high pressure and then sintered in an alumina crucible at 1200 °C for 10 h. Er^{3+}(0.5 at.%):$G_{0.7}Y_{0.3}SO$ polycrystalline material formed by solid-state reaction was then charged into an iridium crucible of 70 mm in diameter and 50 mm in height for crystal growth. The seed cut from Gd_2SiO_5 (GSO) crystal is along the *b* direction. A pulling rate of 1.0–3.0 mm/h and rotation rate of 16–20 rpm were adopted during

* Corresponding author at: Key Laboratory of Materials for High Power Laser, Shanghai Institute of Optics and Fine Mechanics, Chinese Academy of Sciences, Shanghai 201800, China. Tel.: +86 2169918719; fax: +86 2169918485.
E-mail address: zhaoguangjun@163.net (G. Zhao).

0925-8388/$ – see front matter © 2011 Elsevier B.V. All rights reserved.
doi:10.1016/j.jallcom.2011.04.091

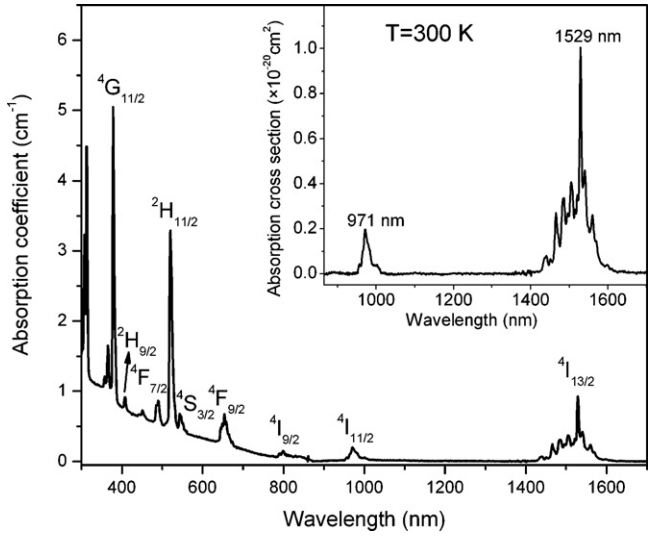

Fig. 1. The RT absorption spectrum of Er^{3+}:$G_{0.7}Y_{0.3}SO$ crystal. The inset shows the absorption cross-sections of bands corresponding to $^4I_{15/2} \rightarrow {}^4I_{11/2}$ and $^4I_{15/2} \rightarrow {}^4I_{13/2}$ transitions.

crystal growth. High purity nitrogen gas was used as the protective atmosphere to prevent oxidation of the iridium crucible. After growth the crystal was cooled to room temperature slowly for more than 36 h to avoid cracking. Transparent crystals 42 mm in length and 31 mm in diameter were thus obtained. The effective segregation coefficient of Er^{3+}, which is equal to 0.94, was measured by inductively coupled plasma atomic emission spectrometer (ICP-AES). The crystal structure of Er^{3+}:$G_{0.7}Y_{0.3}SO$ crystal was checked by XRD (Cu target, Kα) measurement. The crystals were ground into fine powder in order to avoid preferred orientations. Diffraction patterns reveal that the crystal structure of Er^{3+}:$G_{0.7}Y_{0.3}SO$ is consistent with the space group $P2_1/c$ and has lattice parameters of $a = 9.12$ Å, $b = 7.04$ Å, $c = 6.77$ Å, $\beta = 107.86^\circ$.

The room temperature (RT) absorption spectra were measured with a Shimadzu UV-3100 spectrophotometer in the range of 300–1700 nm. Infrared photoluminescence (PL) spectra were measured in a spectral range between 800 and 1700 nm using Jobin-Yvon DSSX-IGA010L InGaAs photo-diode. Light from a 450 W Xenon lamp was used to excite the crystals. The spectrophotometer resolution was 0.2 nm in the infrared (IR) and 0.5 nm in the ultraviolet–visible (UV–vis). Luminescence decay curves were excited by pulses delivered by OPO and recorded using Tektronix Model TDS 3052 digital oscilloscope.

3. Results and discussion

3.1. Absorption spectra and Judd–Ofelt theory analysis

Fig. 1 shows the RT absorption in the 350–1650 nm spectral region of Er^{3+} in $G_{0.7}Y_{0.3}SO$. The spectrum was calibrated in units of absorption coefficient (cm^{-1}) to facilitate the comparison of absorption intensities. It can be seen that it consists of a number of groups of lines corresponding to transitions between the ground state $^4I_{15/2}$ and higher energy states inside the $4f^{11}$ electronic configuration of Er^{3+} ion whereas, the most intense bands related to transitions $\Delta J = 2$ and assigned to the $^4I_{15/2} \rightarrow {}^2H_{11/2}$ (520 nm) and $^4I_{15/2} \rightarrow {}^4G_{11/2}$ (378 nm) ones are in the visible. It is noteworthy that a base absorption line monotonously rises with increasing wavelength in blue and ultraviolet region, which are probably due to several kinds of defect centers. The nature of such bands has not been studied yet. A systematical study of these defects is required in order to improve the technique of growth of $G_{0.7}Y_{0.3}SO$ crystals. However, this is not the goal of the present work.

Transition intensities of Er^{3+} ions in the $G_{0.7}Y_{0.3}SO$ crystal were analysed in the framework of the Judd–Ofelt phenomenological model [11,12]. Then the branching ratios of various transitions from excited state to the ground state and the radiative lifetimes of the levels can be estimated. The measured line strengths of Er^{3+} bands in the $G_{0.7}Y_{0.3}SO$ crystalline host were evaluated by means

Table 1
Measured and calculated line strengths for Er^{3+} in $G_{0.7}Y_{0.3}SO$ crystalline host as well as the intensity parameters Ω_t. (ED-electric dipole contribution, MD-magnetic dipole contribution.).

Transition from $^4I_{15/2}$	Energy	Line strength S ($\times 10^{-20}$ cm^2)		Residual
	ν (cm^{-1})	S_{exp}	S_{cal}	ΔS ($\times 10^{-20}$ cm^2)
$^4I_{13/2}$	6476	2.323	1.566 (ED) 0.761 (MD)	0.001
$^4I_{11/2}$	10,309	0.486	0.514	−0.028
$^4I_{9/2}$	12,516	0.143	0.249	−0.105
$^4F_{9/2}$	15,291	1.199	1.159	0.041
$^4S_{3/2}$	18,416	0.413	0.200	0.213
$^2H_{11/2}$	18,774	4.584	4.590	−0.005
$^4F_{7/2}$	20,388	0.705	0.770	−0.066
$^4F_{5/2} + {}^4F_{3/2}$	22,466	0.220	0.317	−0.097

$\Omega_2 = 5.52 \times 10^{-20}$ cm^2, $\Omega_4 = 1.38 \times 10^{-20}$ cm^2, $\Omega_6 = 0.91 \times 10^{-20}$ cm^2. *RMS* $= 0.12 \times 10^{-20}$ cm^2.

of numerical integration of the RT absorption bands employing the equation:

$$S^{exp}(J \rightarrow J') = \frac{3hc(2J+1)}{8\pi^3 e^2} \cdot \frac{9n}{(n^2+2)^2 N_0} \cdot \frac{\ln 10}{\bar{\lambda} L} \cdot \int_{J-J'} \mathrm{OD}(\lambda) d\lambda \quad (1)$$

where J and J' represent the total angular momentum quantum numbers of the initial and the final manifold states, n denotes the refractive index of $G_{0.7}Y_{0.3}SO$ crystal, N_0 means the density of dopant ions, L is the thickness of the sample, OD (λ) is the measured optical density, h is Planck's constant, m, e and c are the electron mass, electron charge and the velocity of light, respectively. The mean wavelength $\bar{\lambda}$ of the corresponding absorption transitions can be calculated according to the relation: $\bar{\lambda} = \int \lambda \mathrm{OD}(\lambda) d\lambda / \int \mathrm{OD}(\lambda) d\lambda$. Eq. (1) was applied to nine bands located in the 6000–23,000 cm^{-1} spectral range. The transitions to close-lying $^4F_{5/2}$ and $^4F_{3/2}$ states were treated together to reduce the experimental uncertainties. On the other hand, the theoretical values of the line strengths can be calculated by the following equation:

$$S_{ed} = \Sigma_{t=2,4,6} \Omega_t \left| \left\langle (S,L)J || U^{(t)} || (S',L')J' \right\rangle \right|^2 \quad (2)$$

The contribution of magnetic dipole to the $^4I_{15/2} \rightarrow {}^4I_{13/2}$ transition was acquired based on the method reported in [13]. The matrix elements $U^{(t)}$, required for the calculation, were taken from Weber's paper [14] for Er^{3+} in LaF_3. Using a least-squares fitting approach, the intensity parameters were found to be ($\Omega_2 = 5.52 \times 10^{-20}$ cm^2, $\Omega_4 = 1.38 \times 10^{-20}$ cm^2, and $\Omega_6 = 0.91 \times 10^{-20}$ cm^2). The measured and theoretically estimated line strengths for Er^{3+}:$G_{0.7}Y_{0.3}SO$ crystals are displayed in Table 1. The root mean square deviation (*RMS*) being an usual measure of fitting quality, amounts to 0.12×10^{-20} cm^2, a value comparable to those encountered during study of other erbium doped materials. The Ω_t parameters estimated for Er^{3+}:$G_{0.7}Y_{0.3}SO$ are roughly comparable to those of Er^{3+}:GSO ($\Omega_2 = 6.17 \times 10^{-20}$ cm^2, $\Omega_4 = 1.88 \times 10^{-20}$ cm^2, and $\Omega_6 = 1.26 \times 10^{-20}$ cm^2 [4]) and slightly higher than the values reported for Er^{3+}:YSO ($\Omega_2 = 2.84 \times 10^{-20}$ cm^2, $\Omega_4 = 1.42 \times 10^{-20}$ cm^2, and $\Omega_6 = 0.82 \times 10^{-20}$ cm^2 [15]). The results imply that $G_{0.7}Y_{0.3}SO$ lattice supply Er^{3+} ions with a crystal-filed environmental similar to that of GSO. Because in the crystal growth process, a GSO crystal (not YSO) was used as the seed, thus $G_{0.7}Y_{0.3}SO$ crystal has similar crystallographic structures to GSO [8]. Furthermore, it is should be noted that a common feature of these systems is a dominant value of the Ω_2 parameter. This peculiarity, encountered in luminescence materials containing erbium ions, is determined by a high intensity of the $^4I_{15/2} \rightarrow {}^2H_{11/2}$ hypersensitive absorption transition [16]. Then the Ω_t parameters were utilized to predict emission properties of the Er^{3+}:$G_{0.7}Y_{0.3}SO$

Table 2
Values of predicted radiative transition rates of ed and md radiation, luminescence branching ratios and radiative lifetime of excited states of Er^{3+} in $G_{0.7}Y_{0.3}SO$ crystal.

$^{S}L_J$	$^{S'}L'_{J'}$	Average wavenumber (cm^{-1})	A_{ed} (s^{-1})	A_{md} (s^{-1})	β	τ_{rad} (μs)
$^4I_{13/2}$	$^4I_{15/2}$	6476	124	61	1	5405
$^4I_{11/2}$	$^4I_{13/2}$	3833	27	19	0.19	4184
	$^4I_{15/2}$	10,309	193		0.81	
$^4I_{9/2}$	$^4I_{11/2}$	2207	1	3	0.01	3788
	$^4I_{13/2}$	6040	60		0.23	
	$^4I_{15/2}$	12,516	200		0.76	
$^4F_{9/2}$	$^4I_{9/2}$	2775	7		0.01	531
	$^4I_{11/2}$	4982	80		0.04	
	$^4I_{13/2}$	8815	94		0.05	
	$^4I_{15/2}$	15,291	1702		0.90	
$^4S_{3/2}$	$^4F_{9/2}$	3125	1		0	514
	$^4I_{9/2}$	5900	72		0.04	
	$^4I_{11/2}$	8107	40		0.02	
	$^4I_{13/2}$	11,940	548		0.28	
	$^4I_{15/2}$	18,416	1284		0.66	

crystal. The radiative transition rates A_{rad}, luminescence branching ratios β and radiative lifetimes τ_{rad} of excited states of Er^{3+} in $G_{0.7}Y_{0.3}SO$ were estimated based on the Judd–Ofelt model. The obtained results are listed in Table 2.

The energy level structure of erbium ions in $G_{0.7}Y_{0.3}SO$ crystals offers pertinent to an effective optical pumping if the $^4I_{13/2} \rightarrow {}^4I_{15/2}$ laser operation at 1.5 μm is considered. From the inset of Fig. 1, two important absorption bands centered at 971 and 1529 nm are found with peak absorption cross-sections of 0.20×10^{-20} cm^2 and 1.02×10^{-20} cm^2, respectively. These two absorption bands favourably match the emission bands of commercially available InGaAs and InP LDs. The 971 nm pumping will populate $^4I_{13/2}$ upper laser level mainly through a nonradiative process $^4I_{11/2} \rightarrow {}^4I_{13/2}$ with a minor contribution of the $^4I_{11/2} \rightarrow {}^4I_{15/2}$ radiative transitions. The heat load generated in the nonradiative process will result in many detrimental effects such as thermally induced stress birefringence and beam distortion due to the highly aberrated thermal lensing [17]. Thus this pumping approach is not suitable for the high power and high repetition rate operation. Fortunately the sketch of resonantly pumping at 1529 nm for the possible Er^{3+}:$G_{0.7}Y_{0.3}SO$ laser system provides an excellent way to overcome this problem. In this method Er^{3+} ions are directly excited to the upper laser level $^4I_{13/2}$ significantly suppressing the heat generation arising from the $^4I_{11/2} \rightarrow {}^4I_{13/2}$ nonradiative transition. The 1529 nm absorption line of Er^{3+}:$G_{0.7}Y_{0.3}SO$ crystal has a full-width at half-maximum (FWHM) of 6 nm larger than that of Er^{3+}:YAG (~1.9 nm@1532 nm [1]), which is an advantage for the broad-emission-band (~10 nm) InP LD pumping.

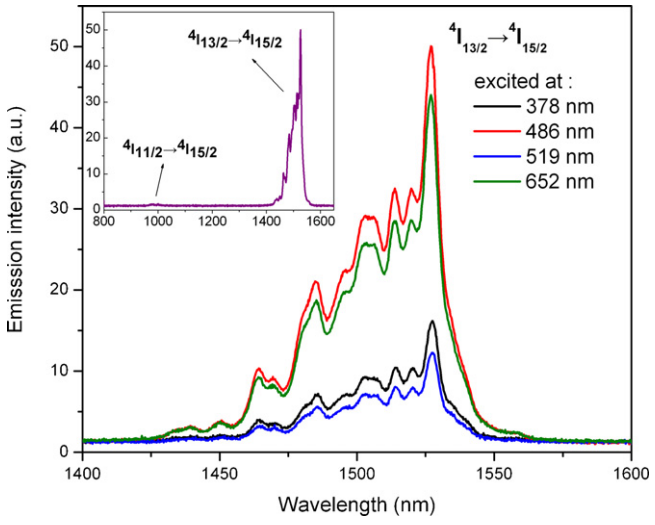

Fig. 2. The RT PL spectra of Er^{3+}:$G_{0.7}Y_{0.3}SO$ crystal related to the transition of $^4I_{13/2} \rightarrow {}^4I_{15/2}$. The inset presents the NIR PL spectrum under the condition of 378 nm excitation.

3.2. PL spectra and stimulated emission cross-section

Fig. 2 displays the infrared photoluminescence spectra excited at 378, 486, 519 and 652 nm at room temperature, respectively, corresponding to the transitions from the $^4I_{15/2}$ state to $^4G_{11/2}$, $^4F_{7/2}$, $^2H_{11/2}$ and $^4F_{9/2}$ excited states. The 1400–1600 nm emission due to the $^4I_{13/2} \rightarrow {}^4I_{15/2}$ transition is generated by the excitation into not only the 378, 486, 519 and 652 nm absorption band but also all the absorption bands in the visible range (Fig. 1) as shown in Fig. 3.

Due to the thermal population among the Stark levels within $^4I_{13/2}$ manifold, the four PL curves related to the $^4I_{13/2} \rightarrow {}^4I_{15/2}$ transition (1400–1600 nm) exhibit broad emission bands with nearly same shapes. The inset shows the near infrared (NIR) spectrum (800–1600 nm) under the condition of 378 nm excitation. Since $^4I_{13/2}$ level of Er^{3+} ions in $G_{0.7}Y_{0.3}SO$ host has a long luminescence lifetime, a great many of Er^{3+} ions relaxed from all the upper excited levels will inhibit at this level. Thus the PL spectrum presents a dominant emission band near 1531 nm corresponding to the $^4I_{13/2} \rightarrow {}^4I_{15/2}$ transition. Whereas most of the Er^{3+} ions at $^4I_{11/2}$ level will relax to $^4I_{13/2}$ level by nonradiative transitions, so only a

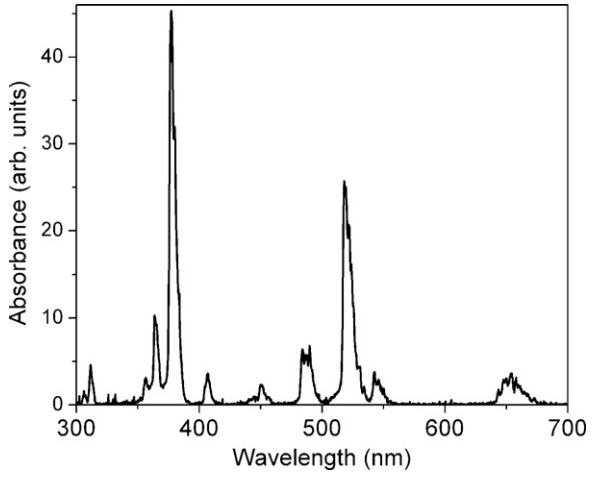

Fig. 3. The PL excitation spectrum for 1528 nm emission of Er^{3+}:$G_{0.7}Y_{0.3}SO$ crystal at RT.

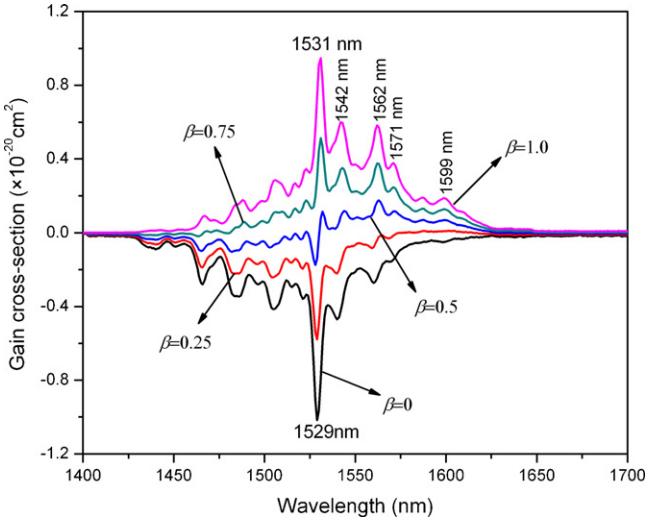

Fig. 4. Stimulated emission cross-section ($p = 1.0$) and gain cross-section spectra estimated for the $^4I_{13/2} \rightarrow {}^4I_{15/2}$ transition.

weak emission band near 970 nm ($^4I_{11/2} \rightarrow {}^4I_{15/2}$) was observed in this spectrum.

The stimulated emission cross-section σ_{em} is recognized as a valuable factor to assess the effectiveness of laser crystals via the quantitative estimation of emission qualities in given spectra related to the $^4I_{13/2} \rightarrow {}^4I_{15/2}$ transition of the Er^{3+}:$G_{0.7}Y_{0.3}SO$ crystal. The emission spectrum in the range of 1400–1700 nm was recorded under the sample excitation by 980 nm cw radiation emitted by InGaAs LD. Using the Fuchtbauer–Ladenburg method [18], the simulated emission cross-section can be estimated by the following equation:

$$\sigma_{em}(\lambda) = \frac{1}{8\pi c n^2 \tau_{rad}} \cdot \frac{\beta \lambda^5 I(\lambda)}{\int \lambda I(\lambda) d\lambda} \quad (3)$$

where n is the refractive index of the sample, c is the speed of light, β is the branching ratio ($\beta = 1$ for the $^4I_{13/2}$ level) and τ_{rad} denotes the radiative lifetime. The stimulated emission cross-section in the region of 1400–1700 nm (the curve with $p = 1.0$ in Fig. 4) are composed of many spectral lines corresponding to transitions between the crystal-field components of the $^4I_{13/2}$ initial state and the $^4I_{15/2}$ terminal level of Er^{3+}:$G_{0.7}Y_{0.3}SO$ crystal. The maximum of the stimulated emission cross-section was found at 1531 nm with a value of 0.95×10^{-20} cm^2. This value is slightly higher than that reported for the Er^{3+}:YAG crystal ($\sigma_{em} = 0.75 \times 10^{-20}$ cm^2 at 1617 nm [1]). To account for the reabsorption losses a gain cross-section is defined as $g(\lambda) = p\sigma_{em}(\lambda) - (1-p)\sigma_{GSA}(\lambda)$, where $p = N_e/N_t$ is the ratio of number of excited ions to the total number of ions and σ_{GSA} is the ground state absorption cross-section. The calculated results with $p = 0$, 0.25, 0.5 and 0.75 are presented in Fig. 4. It is inferred that the potential laser generation in the $^4I_{13/2} \rightarrow {}^4I_{15/2}$ transition of the Er^{3+}:$G_{0.7}Y_{0.3}SO$ is expected to occur at 1562 nm. With the inversion parameter $p = 0.5$, the gain cross-section reaches 0.18×10^{-20} cm^2, which is larger than the other emission peaks such as 1531, 1542, 1571 and 1599 nm. For a comparison, the maximal value of gain coefficient for $p = 0.5$ of the $^4I_{13/2} \rightarrow {}^4I_{15/2}$ emission in Er^{3+}:GSO amounted to $g = 0.24 \times 10^{-20}$ cm^2 at $\lambda = 1560$ nm.

3.3. Excited state relaxation dynamics

Fig. 5(a) and (b) shows the luminescence decay curves for the $^4I_{13/2}$ and $^4I_{11/2}$ levels of Er^{3+}:$G_{0.7}Y_{0.3}SO$ crystal at room temperature, respectively, and the insets present the fitting data in the logarithmic scales. It can be seen that both curves have nearly

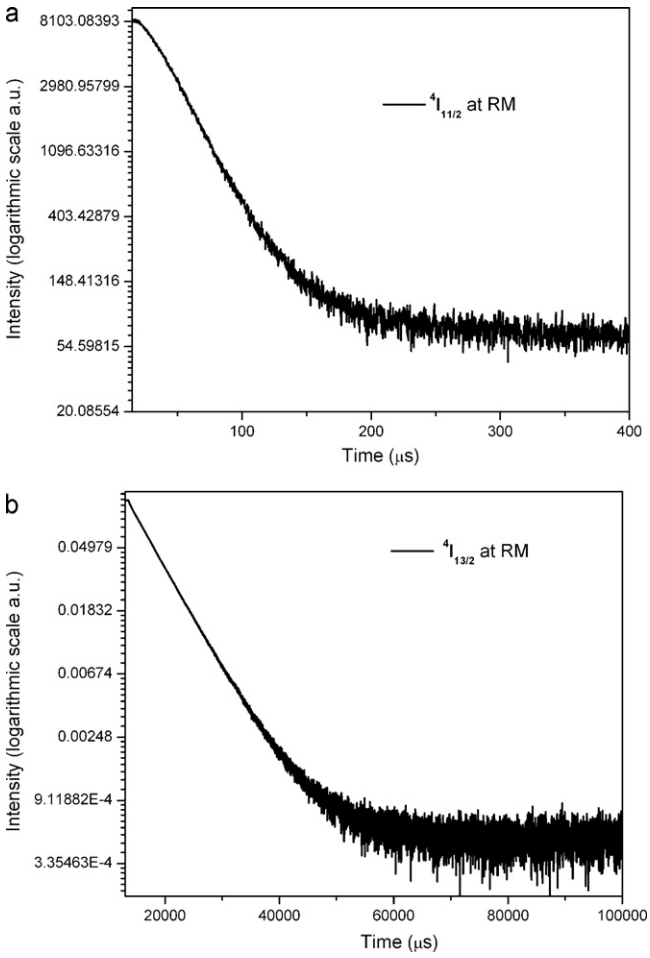

Fig. 5. Luminescence decay curves of $^4I_{11/2}$ and $^4I_{13/2}$ levels of Er^{3+}:$G_{0.7}Y_{0.3}SO$ crystal at room temperature.

single exponential behaviors. Due to the relatively low energy gap (~3800 cm^{-1}) between $^4I_{11/2}$ and $^4I_{13/2}$ levels, many nonradiative transitions including multiphonon relaxations and ion-ion interactions occur between such two levels. Thus the measured luminescence lifetime of $^4I_{11/2}$ level (27 μs) is greatly shorter than the radiative lifetime (4.2 ms). This nature will effectively suppress the upconversion effect occurring at $^4I_{11/2} \rightarrow {}^4S_{3/2}$ or $^4I_{11/2} \rightarrow {}^2H_{11/2}$ [19], and it is very beneficial to realization of population inversion at $^4I_{13/2}$ level under the condition of 980 nm InGaAs LD pumping. However, the measured luminescence lifetime of $^4I_{13/2}$ level (~6.0 ms) is longer than the calculated radiative lifetime (5.4 ms). Maybe it is attributed to the radiative trapping effect [15] because a relatively thick sample (~5 mm) was used for the lifetime measurement. It is noticeable that the $^4I_{13/2}$ lifetime of Er^{3+}:$G_{0.7}Y_{0.3}SO$ is comparable to that of Er^{3+}:YAG (~7.6 ms [20]) which means Er^{3+}:$G_{0.7}Y_{0.3}SO$ crystal also has good energy storage capability facilitating to obtain high power and high repetition rates of 1.5 μm laser output.

4. Conclusions

The Er^{3+}:$G_{0.7}Y_{0.3}SO$ single crystal has been grown by the Czochralski technique. The effective segregation coefficient of Er^{3+} in the $G_{0.7}Y_{0.3}SO$ host is equal to 0.94. The XRD data show that this crystal has a crystalline structure similar to that of GSO and the cell parameters are $a = 9.12$ Å, $b = 7.04$ Å, $c = 6.77$ Å, $\beta = 107.86°$. The

absorption spectrum and PL spectra were measured at room temperature. The radiative rates and branching ratios of Er^{3+} ions from one excited state to all the lower levels were estimated by using the Judd–Ofelt method. The effective intensity parameters Ω_2, Ω_4, and Ω_6 were obtained to be 5.52, 1.38 and 0.91×10^{-20} cm^2, respectively, which are roughly comparable to those of Er^{3+}:GSO. The interesting absorption band corresponding to the radiation of InGaAs LD are located at around 971 nm with a cross-section of 0.20×10^{-20} cm^2, and it is noteworthy that the 1529 nm absorption band ($\sigma_{GSA} = 1.02 \times 10^{-20}$ cm^2) related to the radiation of InP LD has a larger FWHM (~6 nm) than Er^{3+}:YAG. The fluorescence lifetimes of the $^4I_{11/2}$ excited state and the upper laser level $^4I_{13/2}$ are measured to be 27 μs and 6.0 ms, respectively. From the gain cross-section curves, it can be found that the gain coefficient in the region of 1530–1620 nm becomes positive when the inversion parameter p reaches 0.5. The results indicated that Er^{3+}:$G_{0.7}Y_{0.3}SO$ crystal can be considered as a promising laser material operating at around 1.5 μm.

Acknowledgements

The authors thank Dr. Xiaodong Xu for fruitful discussion. This work is financially supported by the National Natural Science Foundation of China no. 90922029.

References

[1] S.D. Setzler, M.P. Francis, Y.E. Young, J.R. Konves, E.P. Chicklis, IEEE J. Sel. Top. Quantum Electron. 11 (2005) 645–657.
[2] M. Eichhorn, Appl. Phys. B-Lasers Opt. 93 (2008) 773–778.
[3] S.D. Setzler, K.J. Snell, T.M. Pollak, P.A. Budni, Y.E. Young, E.P. Chicklis, Opt. Lett. 28 (2003) 1787–1789.
[4] X. Xu, G. Zhao, F. Wu, W. Xu, Y. Zong, X. Wang, Z. Zhao, G. Zhou, J. Xu, J. Cryst. Growth (2008) 1009–1039, doi:10.1016/j.jcrysgro.2007.
[5] K. Spariosu, M. Cashen, R.A. Reeder, V. Leyva, R. Equall, Free-Space Laser Commun. VI 6304 (2006) U116–U124.
[6] L. Fornasiero, K. Petermann, E. Heumann, G. Huber, Opt. Mater. 10 (1998) 9–17.
[7] Y. Ding, G. Zhao, X. Xu, J. Cryst. Growth 312 (2010) 2103–2106.
[8] L.H. Zheng, J. Xu, L.B. Su, W. Ryba-Romanowski, R. Lisiecki, F. Wu, Appl. Phys. B-Lasers Opt. 100 (2010) 493–498.
[9] L.S. Qin, H.Y. Li, S. Lu, D.Z. Ding, G.H. Ren, J. Cryst. Growth 281 (2005) 518–524.
[10] J. Du, X.Y. Liang, Y. Xu, R.X. Li, Z.Z. Xu, C.F. Yan, G.J. Zhao, L.B. Su, J. Xu, Opt. Express 14 (2006) 3333–3338.
[11] B.R. Judd, Phys. Rev. 127 (1962) 750.
[12] G.S. Ofelt, J. Chem. Phys. 37 (1962) 511.
[13] W.T. Carnall, P.R. Fields, K. Rajnak, J. Chem. Phys. 49 (1968) 4412.
[14] M.J. Weber, Phys. Rev. 157 (1967) 262.
[15] C. Li, C. Wyon, R. Moncorge, IEEE J. Quantum Electron. 28 (1992) 1209–1221.
[16] C. Bertini, A. Toncelli, M. Tonelli, E. Cavalli, N. Magnani, J. Lumin. 106 (2004) 235–242.
[17] J.W. Kim, D.Y. Shen, J.K. Sahu, W.A. Clarkson, IEEE J. Sel. Top. Quantum Electron. 15 (2009) 361–371.
[18] B.F. Aull, H.P. Jenssen, IEEE J. Quantum Electron. 18 (1982) 925–930.
[19] S.L. Zhao, Y.B. Hou, X.J. Pei, Z. Xu, J. Rare Earths 23 (2005) 657–661.
[20] J. Koetke, G. Huber, Appl. Phys. B-Lasers Opt. 61 (1995) 151–158.